Asphaltene fractionation based on adsorption onto calcium carbonate: Part 3. Effect of asphaltenes on wax crystallization

Jost Ruwoldt[1*], Sreedhar Subramanian[1], Sébastien Simon[1], Hans-Jörg Oschmann[1], Johan Sjöblom[1]

[1]Ugelstad Laboratory, Department of Chemical Engineering, NTNU, N-7491 Trondheim, Norway

[*]Corresponding author e-mail: jost.ruwoldt@ntnu.no

Keywords: Asphaltene fractionation, paraffin wax, wax crystallization, isothermal titration calorimetry (ITC), cross polarized microscopy (CPM), differential scanning calorimetry (DSC)

Graphical Abstract

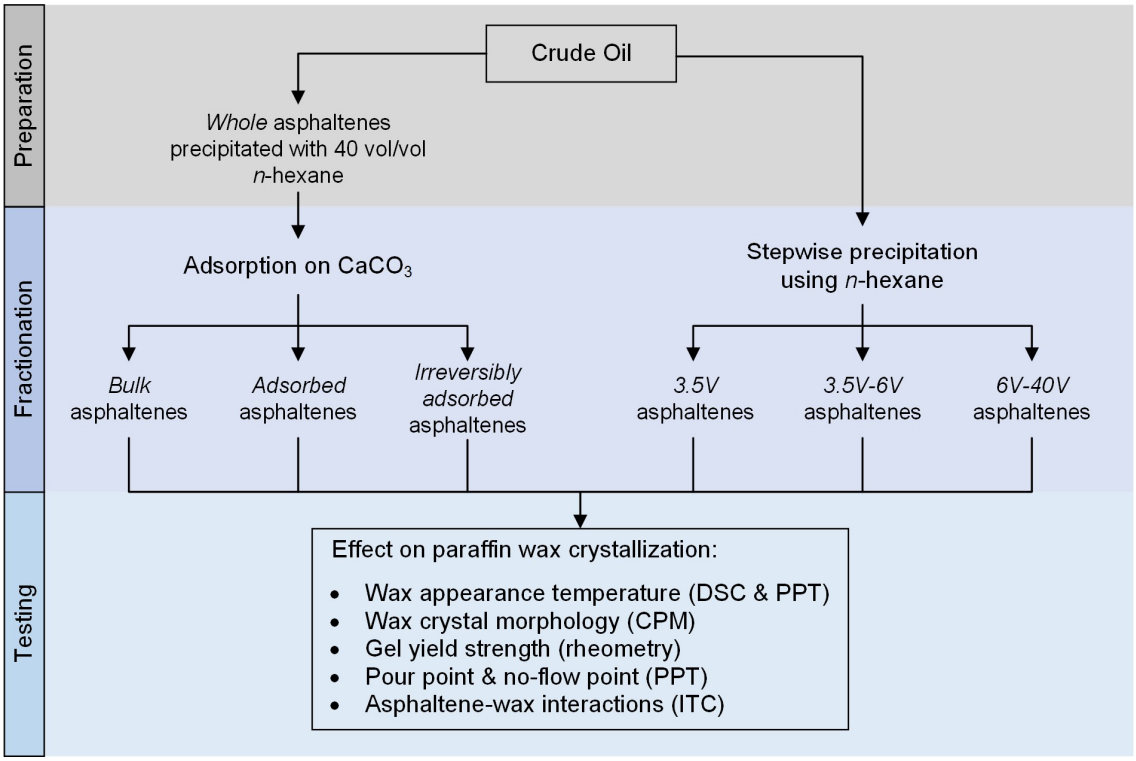

Abstract

Asphaltenes fractionation procedures were developed and tested in two preceding articles (doi: https://doi.org/10.1016/j.colsurfa.2016.02.011, doi: https://doi.org/10.1016/j.colsurfa.2016.11.035), and asphaltene fractions were characterized in terms of composition, adsorption and self-aggregation properties. In this article, the effect of asphaltene fraction on wax crystallization was studied. Asphaltene fractionation on calcium carbonate was developed further to a column separation procedure, which yielded asphaltene fractions with even larger differences according to FTIR analysis. Wax crystallization was studied using differential scanning calorimetry (DSC), cross-polarized microscopy (CPM), rheometry, and pour point tests (PPT). Asphaltenes were found to change wax crystal morphology and decrease gel yield strength with increasing concentration. The effect on wax appearance temperature (WAT) was generally less. The greatest effect on WAT and pour point was made by *bulk* asphaltenes, which is the lowest polarity fraction from separation on calcium carbonate. *Irreversibly adsorbed* asphaltenes, containing significant amounts of carbonyl, carboxylic or derivative groups, induced the largest changes in wax crystal morphology. Still, high pour point and gel yield

strength indicated low performance for this fraction. Overall, wax inhibition performance tended to be best for asphaltene fractions with low solubility and mixed functional groups. In isothermal titration calorimetry (ITC), unfractionated *whole* asphaltenes interacted more strongly with crystallized wax than asphaltene fractions *bulk* and *irreversibly adsorbed*. The findings indicate that wax crystallization is influenced the most by an ensemble of asphaltenes with different functional groups, rather than groups with more distinct properties.

1. Introduction

Current trends in crude oil production are towards higher depths, harsher environments, and increased field complexity. These trends can aggravate flow assurance challenges imposed by paraffin wax in the crude oil. Crystallized wax can cause issues both downhole and topside, which include flow reduction or plugging due to wax deposition, increased fluid viscosity, and restartability issues because of the formation of high strength wax-oil gels [1]. Different thermal, mechanical, and chemical methods are usually taken for wax control, in particular the use of chemical additives such as wax inhibitors (WI) and pour point depressants (PPD) [2, 3]. As new PPDs, the use of fractionated asphaltenes has been suggested [4]. A positive influence on gelation and gel yield strength of waxy crude oils has been attributed to asphaltenes [4-6]. Moreover, several patents exist for the use of asphaltenes as pour point depressants for shale oil [7-9]. In two preceding publications, asphaltenes were fractionated via newly developed procedures that involved asphaltene adsorption on calcium carbonate, as well as stepwise precipitation from bulk [10, 11]. This article is a continuation of previous work, where the fractionation on calcium carbonate was developed further to a column separation procedure that yields asphaltene fractions with even larger property differences. The primary objective was to study the influence of various asphaltene fractions on a model waxy oil. This allows cross referencing of asphaltene properties from current and previous characterizations with their effect on wax crystallization. The goal is to determine which asphaltene characteristics are most crucial during wax crystallization, and hence improve the understanding of asphaltene-wax interactions.

Paraffin wax is a natural constituent of crude oil, which is defined as mostly straight, ring formed, and branched alkanes with 18 or more carbon atoms [1]. Wax crystallization is reported to take place in three steps, which are (i) nucleation, (ii) growth, and (iii) agglomeration [12]. The wax appearance temperature (WAT) is defined as the highest temperature, at which the crystallization of wax can be observed [13]. As the wax crystals grow in size, three dimensional interlocking of the crystals facilitates the formation of a solid like gel [14]. Paraffin wax crystals formed in organic solvents can exhibit plate shapes, needle shapes, and malcrystalline or dendrite like masses [15, 16]. The waxes can be grouped into macrocrystalline and microcrystalline waxes, depending on the crystal shape [17]. Macrocrystalline wax has been reported to largely consist of low molecular weight *n*-alkanes that form predominantly plate shaped crystals with large hydrodynamic radii. Microcrystalline wax is considered to contain significant amounts of high molecular weight *iso*-alkanes and *cyclo*-alkanes, leading to compact and round crystal morphologies with smaller diameters. As a consequence, macrocrystalline wax generally leads to the formation of strong gels, whereas microcrystalline wax accounts for in comparison weak gels [18].

The temperature at which a liquid loses its ability to freely flow due increasing amounts of precipitated wax is referred to as pour point, as defined by ATSM D97 [19]. A pour point depressant (PPD) consequently refers to chemical additives, which can decrease the pour point. The term wax inhibitor (WI) will be used in a more general context in this study. It refers to chemical additives that can alleviate challenges associated with paraffin wax crystallization via one or more functionalities. PPDs function as crystal modifying substances through co-precipitation with the wax [20-22]. PPD polymers provide

spatial hindrances during continued crystals growth, leading to the formation of distorted and more compact crystal shapes with lower hydrodynamic radius. This can further result in particle dispersions with lower viscosity, wax-oil gels of lower yield strength, and prevention or delay of the formation of a solid like gel, a process also referred to as pour point depression. Asphaltenes have been noted to predominantly interact with the more polar or aromatic groups of a PPD [17]. In waxy crude oils, the presence of asphaltenes has been reported to enhance as well as diminish the effect of WIs and PPDs [23, 24]. For example, synergistic effects between asphaltenes and maleic anhydride co-polymers (MAC) as well as ethylene-vinyl acetate copolymer (EVA) have been reported [25-27].

Asphaltenes have been reported to be natural PPDs by many authors [5, 6, 23, 25-34]. Still, the effect of asphaltenes has been discussed contradictorily [35]. Some authors state no synergistic interactions between wax and asphaltenes [36], and other authors report asphaltenes aggravating issues associated with paraffin wax [24, 37]. Asphaltenes are defined via solvent properties, being insoluble in low molecular weight *n*-alkane solvents [38]. Due to this definition, asphaltenes can have greatly varying composition and properties depending on the crude oil of origin, which would in turn account for the contradicting reports. However, most reports agree on the following effects that asphaltenes can have on paraffin wax crystallization:

1. Asphaltenes can serve as nucleation sites for wax crystals, which can increase WAT [37], but also lead to more finely dispersed wax crystals [6, 23].
2. Asphaltenes can co-crystallize with wax, which can alter crystal morphology and improve crude oil rheology [6, 29, 35, 39].
3. It is mainly the aliphatic part of asphaltenes, which interacts with paraffin wax [29, 39, 40].
4. The dispersion degree of asphaltenes plays a crucial role during wax crystallization [5, 30, 31].

Several authors have investigated the effect of asphaltene properties on wax crystallization by using either asphaltenes originating from different crude oils [24, 29] or fractionated asphaltenes [4, 6, 34]. In two of these cases, asphaltene fractionation has been conducted by dissolving asphaltenes in dichloromethane (DCM) and inducing stepwise precipitation with pentane [34, 41]. In one case, asphaltenes were fractionated on silica gel and via reverse phase chromatography [4]. The authors concluded that low polarity asphaltenes and the abundance of alkyl chains accounted for better pour point depression [4, 6, 29, 34]. High polarity asphaltenes were reported to have less of an effect on wax crystallization.

2. Experimental Section

2.1. Materials

An additive free crude oil from the Norwegian continental shelf was used for asphaltene precipitation, which is identical to the crude oil used in the two preceding studies [10, 11]. Macrocrystalline wax was acquired as 5405 Sasolwax from Sasol, Germany. Composition and properties of the wax can be found in literature [42]. Solvents for model oil systems were obtained as xylene isomer blend (VWR, ≥98.5%, reagent grade) and *p*-xylene (Sigmaaldrich, 99%, ReagentPlus®). Asphaltenes were extracted with *n*-hexane (VWR, ≥97%, HPLC-grade). Asphaltene fractionation was performed with precipitated calcium carbonate (Speciality Minerals Inc., USA), chloroform (VWR, 99.0-99.4%, analytical reagent), toluene (Sigmaaldrich, 99.8%, anhydrous), dichloromethane (DCM) (Sigmaaldrich, 99.8%, anhydrous, 40-150 ppm amylene as stabilizer), hydrochloric acid (Merck, 37%), and milli-Q water.

2.2. Sample Preparation

Solutions containing paraffin wax, also referred to as waxy model oils or model system, were prepared by first weighing the solid(s), and then adding the required amount of liquid solvent. After preparation,

the solution was heated to at least 20 °C above WAT for at least 30 min prior to use, to ensure complete dissolution of all solids. Samples containing asphaltenes were sonicated for at least 30 min before use. Crude oil was heated at 60 °C for 1 h, and shaken thoroughly before sampling to ensure homogeneity of the sample.

2.3. Asphaltene Extraction

Asphaltenes, termed *whole* asphaltenes, were obtained by mixing the crude oil with 40 vol/g *n*-hexane and stirring for at least 24 h at ambient conditions. The resulting mixture was filtered with 0.45 μm HVLP-type Millipore filter membrane and the filter cake was rinsed with *n*-hexane until the filtrate was entirely clear. Filter plus *whole* asphaltenes were then dried under nitrogen atmosphere for at least 24 h. The final yield accounted for 2.5 ± 0.1 wt% of the original crude oil.

2.4. Asphaltene Fractionation

2.4.1. Fractionation Based on Bulk Precipitation

The detailed procedure for asphaltene fractionation via bulk precipitation is described in a preceding publication [11]. In short, *n*-hexane was added to crude oil in three steps, following a dilution of 3.5, 6, and 40 volumes of *n*-hexane per gram crude oil. After each step, asphaltenes were recovered via filtration with a 0.45 μm Millipore filter. The filtrate was washed with 50 ml *n*-hexane and dried under nitrogen atmosphere. The fractions *3.5V*, *3.5-6V*, and *6-40V* asphaltenes were obtained by this procedure, where the prefix refers to the dilution ratio of crude oil with *n*-hexane in vol/g.

2.4.2. Fractionation Based on Adsorption on Calcium Carbonate

The fractionation on calcium carbonate was based on the previous work done by Subramanian et al. [10]. Minor adjustments to the fractionation procedure were made by using a fixed bed column, and using chloroform instead of tetrahydrofuran (THF) to obtain *adsorbed* asphaltenes. The reason for a change in solvent was that retention times were considerably higher using a column than the original batch procedure, and THF was found to oxidize the asphaltenes after long exposure.

A flow diagram of the column separation procedure is shown in Fig. 1. Asphaltene solution was prepared as 4 g/l *whole* asphaltenes in toluene. The solution was sonicated for 30 minutes and then stirred overnight. The next day, the asphaltene solution was filtered through a 0.45 µm HVLP filter before transferring it to the packed bed column consisting of calcium carbonate (mean particle size = 0.7 µm, BET area = 14.7 m^2/ mg) . A ratio of at least 130 g/g calcium carbonate per *whole* asphaltenes was used to provide sufficient surface area for adsorption.

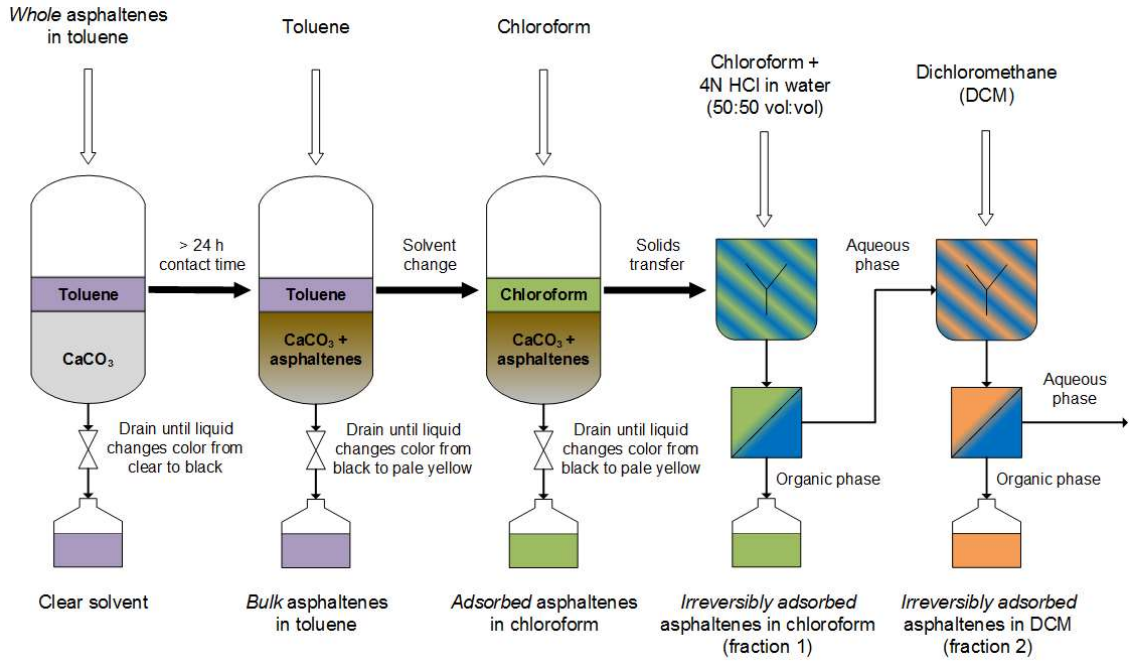

Fig. 1. Flow diagram of asphaltene fractionation of calcium carbonate

The asphaltene solution was allowed to flow through the column, and dropwise eluted by using a drain valve, thereby allowing sufficient time for contact between the asphaltenes and the calcium carbonate packing. Fresh toluene was added to the column at periodic intervals to ensure that the column did not become dry. Once the solvent drained at the bottom of the column changed color from black to pale yellow as shown in Fig. 2, the end of the first elution step was marked. All asphaltene in toluene solution collected until this point was labelled as bulk asphaltene solution. In the next stage, chloroform was used as the solvent for extraction of asphaltenes from the packed column. The same procedure as for *bulk* asphaltenes was repeated. The column was replenished with chloroform and drained at the bottom until the drained solvent color again changed from black to pale yellow. The collected asphaltene solution in chloroform is labelled as *adsorbed* asphaltene solution. The remaining asphaltenes present in the column were extracted by dissolving it in an equivolume mixture of chloroform and 4 N HCl solution. The organic and aqueous phases were separated. The organic layer containing asphaltenes was thus labelled *irreversibly-adsorbed* asphaltenes (fraction 1). Some asphaltenes were found to remain in the aqueous layer, and this was further extracted using DCM. This fraction was labelled as irreversibly adsorbed asphaltenes (fraction 2). Fraction 1 and fraction 2 of *irreversibly adsorbed* asphaltenes were treated individually during characterization, but mixed together as one fraction to study the effect on wax crystallization. All asphaltene solutions were filtered separately using a 0.45µm filter, before being concentrated in a rotary evaporator followed by drying under nitrogen stream at up to 70°C using a block heater (Grant UBR).

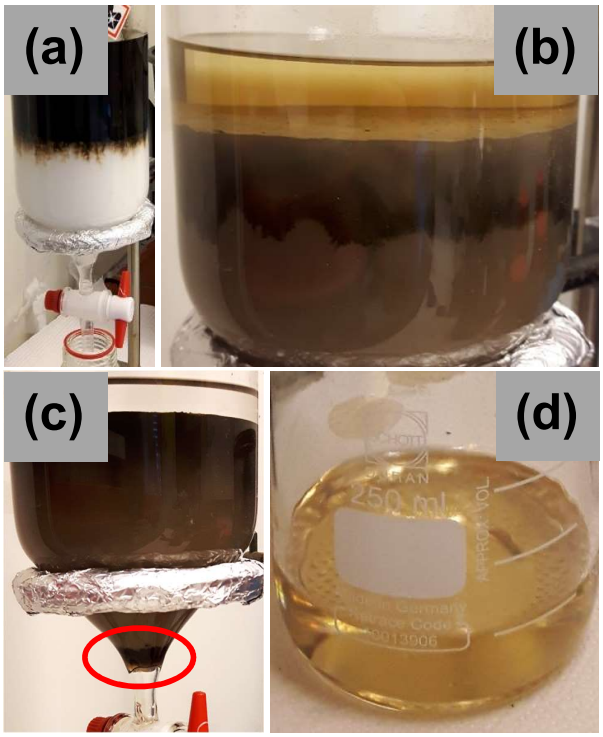

Fig. 2. Asphaltene fractionation on calcium carbonate: (a) Introduction of *whole* asphaltenes in toluene onto the column, (b) column during the elution with chloroform, (c) column after removal of *adsorbed* asphaltenes (contrast and brightness adjusted), where the glass wool is encircled in red, and (d) pale yellow eluate that marks the end of an elution step.

2.4.3. Asphaltene Characteristics

Extensive characterization of asphaltenes fractionated by both adsorption on calcium carbonate and bulk precipitation has been performed earlier [10, 11]. These characterization techniques include the use of elementary analysis, Fourier-transformed infrared spectrometry (FTIR), precipitation onset measured with near-infrared spectroscopy (NIR), adsorption on stainless steel via quartz crystal microbalance (QCM), and self-association in isothermal titration calorimetry (ITC). Among the bulk precipitated asphaltene fractions, the *asphaltene 3.5V* sub-fraction was found to contain higher amount of oxygen compared to fractions *3.5V-6V* and *6V-40V* [11]. Other properties of asphaltene sub-fractions described in previous work include higher self-association (ITC, NMR) and lower solubility characteristics (NIR) among *irreversibly-adsorbed* asphaltenes, along with a significantly higher ability to adsorb on stainless steel [10, 11]. Extended work on the more detailed composition of all sub fractions was also done based on NMR and mass spectrometry techniques [43].

In this work, elemental composition (C, H, N, O, S) and metal content (Fe, Ni, V, Ca, Na, K) for the asphaltene sub-fractions obtained from the modified column method described in section 2.4.2 was determined by Laboratory SGS Multilab (Evry, France) [10]. Similarly, the FTIR spectra of column separated asphaltene sub-fractions was recorded using a Tensor 27 spectrometer (Bruker Optics) equipped with a Bruker Golden Gate diamond Attenuated Total Reflection (ATR) cell.

2.5. Differential Scanning Calorimetry (DSC)

Experiments were conducted on a DSC Q2000 from TA Instruments. Instrument calibration was done by measuring the melting of indium. Prior to experiment, 10 to 20 mg sample were loaded in the sample pans and sealed hermetically. Before and after each experiment, the sample pans were weighed to ensure that no sample loss due to evaporation had occurred. Before each measurement, the sample was heated

to at least 40 °C above WAT for at least 2 min, to erase the thermal history. The WAT was determined according to a previously published procedure [44]. In this procedure, the baseline is approximated by linear least squares and the WAT is defined as exceeding a threshold value, set as 3.291 times the standard deviation of experiment data from the linear approximation. Four measurements were done for each cooling rate and sample. Extrapolation to a zero cooling rate was done from WAT data with cooling rates of 2 to 0.5 °C/min.

2.6. Rheometry and Gel Breakage

Gel breakage measurements were conducted on an Anton Paar Physica 301. The rheometer was equipped with a 4 cm diameter 2° cone and plate geometry, which had been sandblasted for providing additional roughness and preventing slippage. A gap size of 0.170 mm was used. Experimental procedures consisted of preheating the sample to more than 20 °C above WAT, and loading it into the rheometer geometry set at 35 °C. Cooling at a rate of 1 °C/min was done until 4 °C, and then kept isothermal for 10 min. The sample was subsequently sheared at a shear rate of 0.1 s^{-1} and the development of shear stress with total strain was recorded. The gel breakage strength was defined as the maximum shear stress, which appeared right after the linear elastic regime. Each measurement was repeated four to six times.

2.7. Cross-Polarized Microscopy (CPM)

To observe changes in wax crystal morphology, cross polarized microscopy (CPM) was applied. A Nikon Eclipse ME600 microscope fitted with a CoolSNAP-Pro camera by Media Cybernetics and cross-polarization filters were used for CPM imaging. A stage micrometer was taken for scaling. The temperature was controlled via a Linkham PE 94 and LTS-120E Peltier system. The samples were filled into glass capillaries with a cross section of 0.3 x 0.03 mm, which were fixated on microscope slides and sealed on both ends with 3M Scotch cyanoacrylate base glue. An air bubble was kept between glue and sample to prevent contamination. The temperature program consisted of heating to 60 °C, keeping isothermal for 15 min, and subsequent cooling at a rate of 1 °C/min to 4 °C. The sample was then kept isothermal, and images were taken within the time frame of 20 to 40 min after reaching 4 °C.

2.8. Pour Point Tester (PPT)

Pour point analyses were done according to ASTM D5985 [45], using a Pour Point Tester (PPT) 45150 from PSL Systemtechnik, Germany. The no-flow point is measured as deflection of the piston located in the sample cell rotating at 0.1 rpm. The pour point can be computed from the no-flow point by rounding up to the nearest multiple of 3 °C. In Fig. 3, the temperature changes during a measurement cycle are exemplarily shown. The wax was re-dissolved by heating to 45 °C between each measurement. The WAT was determined analogous to DSC experiments in section 2.5, i.e. the sample temperature was approximated linearly and the WAT was defined as exceeding the confidence interval (as 3.291 times the standard deviation) around the baseline on a 10 °C interval. The slope of the baseline resembles the applied cooling rate and was 3.9 °C/min on average when detecting WAT.

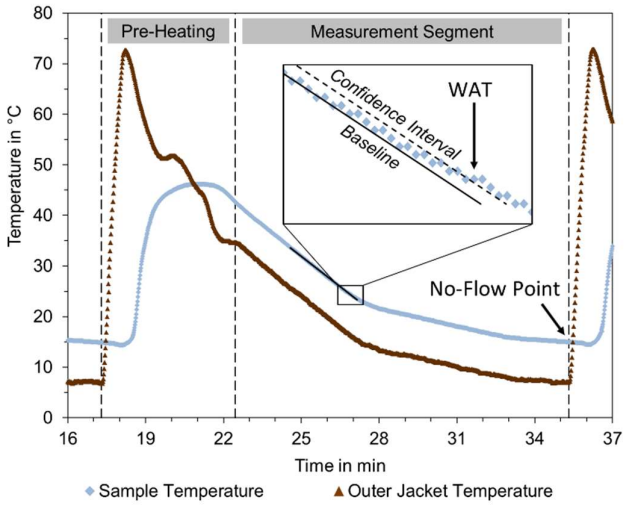

Fig. 3. Exemplary PPT data for 1000 ppm *whole* asphaltenes and 10 wt% macrocrystalline wax in p-xylene. The no-flow point marks the end of each measurement segment. The no-flow point is determined according to ASTM D5985 as deflection of a piston in the rotating sample beaker [45]. The WAT is determined as exceeding the confidence interval around the linear baseline approximation.

2.9. Isothermal Titration Calorimetry (ITC)

ITC experiments were performed on a NANO ITC Standard volume from TA Instruments. Both sample and reference cell have a volume of 1 ml. The reference cell was filled with bulk solvent of xylene isomer blend. The instrument was calibrated via measuring the reaction heat for defined titrations of Tris-base with HCl. Before each experiment, the instrument was equilibrated to a baseline drift of less than 0.1 µW, which took approximately 30 to 60 min. Titrations were done in 25 injections of 10 µl using a 250 µl syringe and stirring at 250 rpm. Injection intervals were set to match the time needed for the heat signal to return to the baseline. Experiments conducted at 35 °C used injection intervals of 5 to 15 min, and experiments conducted at 20 °C involving paraffin wax had injection intervals of 60 min. Data evaluation was done in the NanoAnalyze software of TA Instruments with automated heat integration of each injection. The interaction heat was calculated as net enthalpy ΔH_{Int}, which is the difference of the measured heat values for the dissociation of asphaltenes ΔH_{Asph}, the dilution or re-dissolution heat of wax ΔH_{Wax}, and combined effects of titrating asphaltenes into wax ΔH_{Total}. The latter three quantities are measured in separate experiments. For each, the heat generated due to friction in the syringe was subtracted, which was obtained from blank xylene into xylene injections. The net enthalpy ΔH_{Int} is then computed via equation (1), in analogy to Wei et al. [46].

$$\Delta H_{Int} = \Delta H_{Total} - (\Delta H_{Asph} + \Delta H_{Wax}) \quad (1)$$

Solvents and solutions for ITC were degassed by sonicating for at least 30 min. Asphaltene solutions were prepared at least one day in advance and stored at room temperature, to ensure that the solutions had stabilized. Wax dispersions were prepared by quenching the hot waxy solution at 20 °C in a temperature controlled bath. As part of the quenching, the dispersion was kept in the bath for a duration of 1 h, shaken vigorously for 5 s after removal, and sonicated for 20 to 30 s before being filled into the ITC sample chamber.

3. Results and Discussion

3.1. Characterization of Asphaltene Fractions

3.1.1. Fractionation Yields

The average yield in percentages from asphaltene fractionation are listed in Table 1. Each value is the average of two to five batches with according standard deviation. The bulk precipitation procedure yielded values close to the target of 20 %, 30 %, and 50 % for the fractions *3.5V*, *3.5V – 6V*, and *6V – 40V* asphaltenes, respectively [11]. The fractionation on calcium carbonate produced yields that are significantly lower for *bulk* and *irreversibly adsorbed* asphaltenes, and higher for *adsorbed* asphaltenes than previously reported [10]. However, the order of magnitude for each fraction yield is very similar. Differences can be explained by changing the procedure from batch to column, and by the substitution of THF with chloroform. Also, a lower percentage of asphaltenes was recovered at the end. One factor contributing to the loss of material is due to glass wool that is used to keep the calcium carbonate in place. Asphaltenes would adsorb on the glass wool, which could not be retrieved in subsequent steps.

Table 1. Average yields of asphaltene fractionation with according standard deviation. The fractionation on calcium carbonate was conducted three times, and the fractionation via bulk precipitation was conducted five times.

Procedure	**Fraction and Yield with Standard Deviation *[wt%]***				**Total Recovered**
Fractionation on calcium carbonate	*Bulk* 38.8 ± 6.8 %	*Adsorbed* 42.7 ± 4.1 %	*Irreversibly Adsorbed* 12.4 ± 0.3 %		93.9 ± 2.8 %
			Fraction 1 9.2 ± 1.1 %	Fraction 2 3.4 ± 1.0 %	
Fractionation via bulk precipitation		*3.5V* 18.2 ± 0.5 %	*3.5V-6V* 34.3 ± 0.1 %	*6V-40V* 47.5 ± 0.1 %	~100%

3.1.2. Elemental Analysis

The elemental and metal composition of the asphaltene sub-fractions obtained from column fractionation method is given in Table 2. The calcium content in all the sub-fractions (*bulk*, *adsorbed* and *irreversibly adsorbed*) is lower than the whole (filtered) asphaltenes, thereby indicating that the samples are not contaminated by $CaCO_3$. The H/C ratio varied over a broader ranger (1.15 – 1.29), with the *irreversibly adsorbed* asphaltene sub-fractions (both 1 and 2) exhibiting a higher aliphatic nature, which is in agreement with previous results [10]. There is a noticeable variation in the oxygen content among the sub-fractions, with *irreversibly adsorbed* asphaltenes exhibiting a much higher content of oxygen. The oxygen content in *irreversibly adsorbed* fractions (4.48% and 3.79%) obtained in the present column fractionation method is comparable with the data reported by Subramanian et al. [10], who obtained an oxygen content of 4.22% in the *irreversibly adsorbed* asphaltene sub-fraction. The *bulk* asphaltenes in column method show the least content of oxygen atoms (1.44%), followed by adsorbed asphaltenes with 2.28%. The *adsorbed* asphaltenes have been enriched in nitrogen and sulfur heteroatoms, as well as metals Ni and V. In conclusion, an evolution of elemental composition from *bulk* to *irreversibly adsorbed* asphaltenes can be seen in terms of H/C ratio and oxygen content.

Table 2. Elemental and metal composition of asphaltene sub-fractions obtained by column fractionation. The mass balance is indicated by a percentage in gain (positive) and loss (negative), and is calculated with respect to *whole* asphaltenes as reported earlier [10].

Element	**Asphaltenes**					**Percentage loss or gain**
	Whole (filtered)	*Bulk*	*Adsorbed*	*Irreversibly adsorbed* Fraction 1	Fraction 2	

C *[wt%]*	86,1	86,1	84,2	81,4	82,9	-4,2
H *[wt%]*	8,40	8,28	8,31	8,39	8,88	-3,6
N *[wt%]*	1,40	1,21	1,52	1,30	1,10	-7,6
O *[wt%]*	1,83	1,44	2,28	4,48	3,77	12,6
S *[wt%]*	2,26	1,80	2,30	1,92	1,94	-13,7
Total *[wt%]*	99,99	98,83	98,61	97,49	98,59	-
H/C Ratio *[-]*	1,171	1,154	1,184	1,237	1,285	-
Fe *[ppm]*	<42	<24	<29	626	<63	-
Ni *[ppm]*	67	59	81	<65	64	-
V *[ppm]*	223	248	278	166	172	8,6
K *[ppm]*	<420	<240	<290	<650	<630	-
Na *[ppm]*	<420	<240	<290	<650	<630	-
Ca *[ppm]*	987	242	<290	<650	<630	-

3.1.3.FTIR Spectroscopy

The FTIR spectra of column fractionated asphaltenes and *whole* asphaltenes are shown in Fig. 4 All asphaltene sub-fractions show similar absorption bands at 2950 cm^{-1} and 2830 cm^{-1}, thereby indicating similar alkyl groups across the fractions. Only the *irreversibly adsorbed* asphaltenes (fractions 1 and 2) show significant absorption at 1700 cm^{-1}, which corresponds to presence of carbonyl, carboxylic or derivative groups. Thus, the IR spectra and elemental analysis indicates that the column procedure has resulted in obtaining asphaltene sub-fractions with more distinct differences, especially in *bulk* and *adsorbed* asphaltenes. The composition of *irreversibly adsorbed* asphaltenes appears to be similar as reported earlier [10, 11].

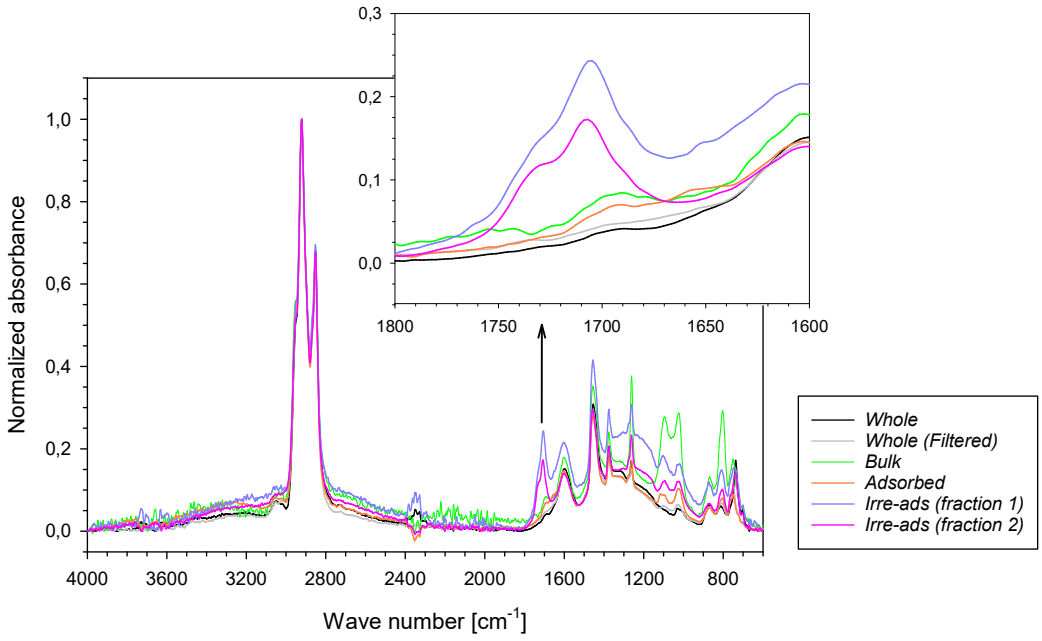

Fig. 4. FTIR spectra of asphaltene sub-fractions

3.2. Effect of Asphaltene Concentration on Wax Crystallization

The influence of *whole* asphaltene dosing was tested on model oil solutions of 10 wt% macrocrystalline wax in xylene with different amounts of asphaltenes. Gel breakage strength, WAT, and pour point were taken as representative performance criteria for the ability of asphaltenes to act as WIs and PPDs.

It has been demonstrated that the gel breakage strength is independent of shear rate, as long as the shear rate is sufficiently low [47]. As depicted in Fig. 5, deviation from the target shear rate could occur in the beginning, but the shear rate was sufficiently close to the target value of 0.1 s^{-1} when gel breakage occurred. Adding *whole* asphaltenes not only decreased the gel breakage strength, but also resulted in gel breakage at lower levels of strain. Also, adhesive breakage can be observed for the sample containing no asphaltenes, which is visible as oscillations of shear stress and shear rate at a strain of 50 % and more. Ideal adhesive breakage is marked by a stick-slip behavior of the gel, which shows as oscillations of the shear stress during continuous shearing [48]. The fact that adhesive breakage has not been observed for samples containing asphaltenes indicates different gel properties and a different gel degradation mechanism.

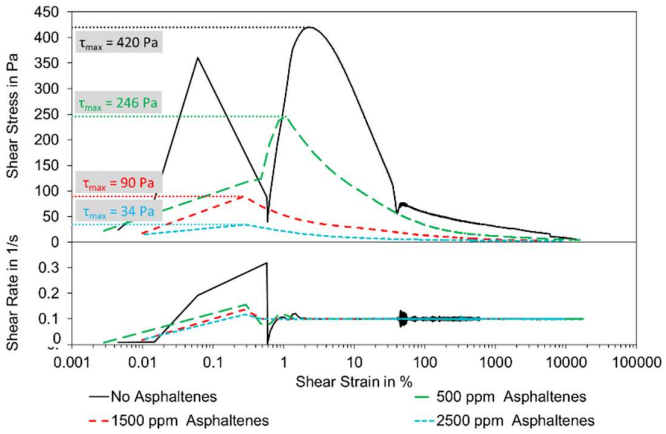

Fig. 5. Stress-strain diagram showing the influence of different amounts of *whole* asphaltenes on gel yield stength of 10 wt% macrocrystalline wax in xylene isomer blend at 4 °C.

Exemplary results of WAT values from DSC experiments are plotted in Fig. 6. The development of WAT with cooling rate can be best described as quadratic parabola, which faces concave upward. However, for cooling rates between 0.5 °C/min and 2 °C/min, the progression of WAT is approximately linear. This cooling rate regime was therefore used for linear extrapolation to an infinitely small cooling rate denoted as WAT_0. Another reason for this extrapolation is that data scattering makes comparison at a single, low cooling rate difficult. Fig. 6 also indicates a decrease in WAT with the addition of more *whole* asphaltenes. As can be seen in Fig. 7, the WAT_0 would decrease until a concentration of 2000 ppm was reached, and increase thereafter. The addition of *whole* asphaltenes therefore appears to improve the solubility of macrocrystalline wax only until a certain point, but not further. In comparison, gel breakage strength decreased for each concentration increase over the entire range tested in Fig. 7.

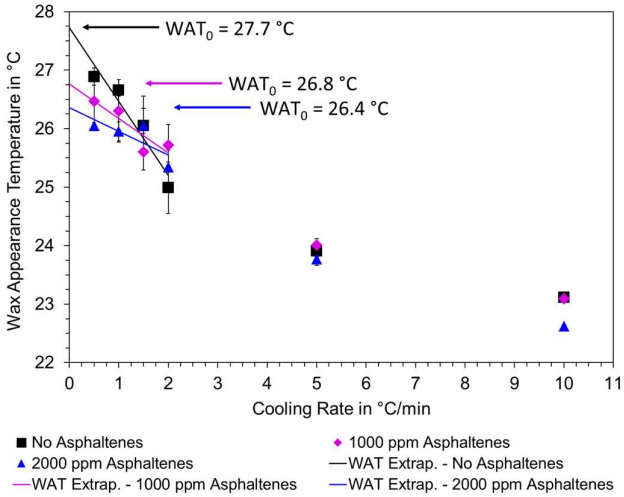

Fig. 6. DSC results for WAT progression with cooling rate for different amounts of *whole* asphaltenes, and 10 wt% macrocrystalline wax in xylene isomer blend. The solid straight lines mark extrapolation to WAT_0 at zero cooling rate. Each point represents the average of four measurements with according standard deviation.

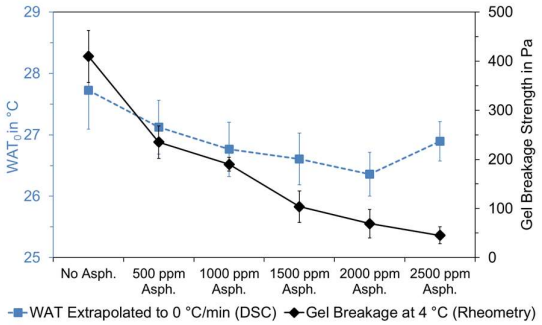

Fig. 7. Influence of amounts of *whole* asphaltene on WAT_0 and gel breakage in a waxy model oil. Measurements were done with *whole* asphaltenes and 10 wt% macrocrystalline wax in xylene isomer blend. The WAT_0 was obtained via linear extrapolation from cooling rates between 0.5 °C/min and 2 °C/min with four measurements per cooling rate, yielding 16 measurements per WAT_0. Gel breakage strength was calculated as the maximum yield stress recorded during gel breakage with four measurements per sample. Error bars represent the standard deviation of each value.

The effect of *whole* asphaltene addition on crystal morphology was investigated via CPM, and results are presented in Fig. 8. CPM imaging of 10 wt% macrocrystalline wax in xylene isomer blend shows lines of different thickness, which are oriented either in parallel and orthogonal to each other, or branched around a common center. These structures account for needle and plate shaped crystals. As the amount of asphaltenes increases, the observed shapes become on average smaller, more compact, and more branched, which indicates whole asphaltenes to act as a crystal modifier. Considering the reduction in gel breakage strength induced by *whole* asphaltene addition in Fig. 7, the morphological changes appear to also reduce the three dimensional interlocking of wax particles. Moreover, the amount of visible wax particles in Fig. 8 increases with increasing asphaltene concentration. In CPM imaging, only the portion of crystals can be seen, which have an orientation that allows for the depolarization of light. The increase in observable wax crystals consequently does not imply an increase in solid wax content, but a diversification of crystal geometry and orientation.

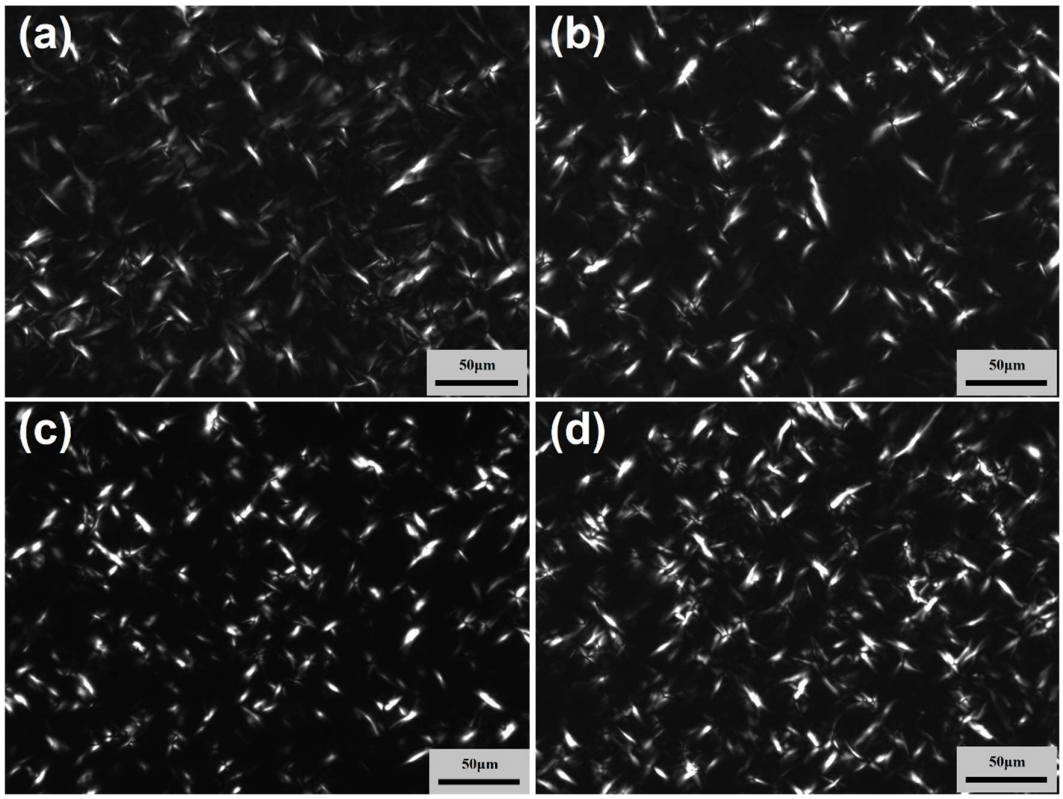

Fig. 8. CPM images of 10 wt% macrocrystalline wax in xylene isomer blend with (a) no additive, (b) 500 ppm, (c) 1500 ppm, and (d) 2500 ppm *whole* asphaltenes.

Fig. 9 shows that the addition of *whole* asphaltenes could decrease the WAT for all samples tested. Still, the WAT decrease became statistically significant only at concentrations of 5000 ppm and more. In comparison to DSC measurements, the scattering of WAT is more pronounced. Also, the WAT obtained from PPT measurements is slightly lower than in DSC of Fig. 7. This is a consequence of the faster cooling rate employed and the fact that the PPT is not designed for WAT determination. Also presented in Fig. 9 is the influence of *whole* asphaltenes on no-flow point, which exhibits better reproducibility than WAT measurements. The No-Flow Point represents an estimate of the pour point with a higher temperature resolution. It increased at 500 ppm *whole* asphaltenes compared to the case with no asphaltenes. For higher asphaltene concentrations, the no-flow point followed a decreasing trend, except for increasing the concentration to 2 wt% *whole* asphaltenes. This shows that the addition of *whole* asphaltenes can have positive as well as adverse effects on the flow-ability of the waxy model oil. The largest reduction in no-flow point from the blank case was 1.5 °C, which is comparably low. Pour point decreases of 30 °C and more are often needed to ensure unobstructed flow in subsea pipelines. It has been stated that high paraffin wax percentages may diminish the possible effect of PPDs [22]. A reduction in wax percentage in the waxy model oils could have improved the sensitivity of no-flow point to asphaltene addition. Still, the wax amount was kept constant at 10 wt% for better comparison between all techniques.

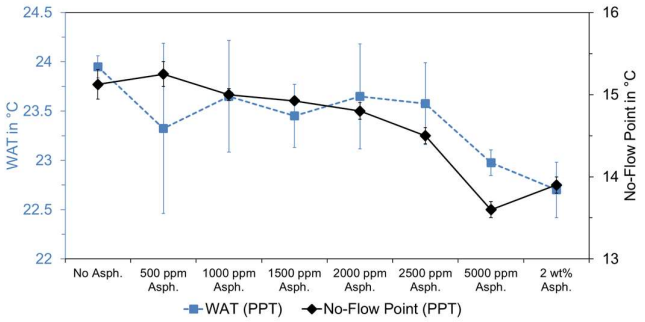

Fig. 9. Influence of different amounts of *whole* asphaltene on WAT and No-Flow Point. Measurements were done with *whole* asphaltenes and 10 wt% macrocrystalline wax in p-xylene using a pour point tester (PPT). Each value represents the average of 2 to 4 measurements with according standard deviation as error bars.

3.3. Effect of Asphaltene Fraction on Wax Crystallization

Asphaltene fractions were tested in model waxy oils with 1500 ppm asphaltenes and 10 wt% wax in xylene. Experiments were set up in such a way, to have all asphaltene fractions present as stable nano-aggregates. This was confirmed by random screening of the mixtures using a microscope and at no point were asphaltene flocculates found. Xylene represents only the aromatic fraction of crude oil neglecting the major constituent, which is saturated and aliphatic in nature. This deviation from real world systems was deemed necessary, because using an aliphatic solvent would result in asphaltene flocculation. These flocculates can be different in properties and quantity depending on asphaltene fraction used, so the conducted experiments would be less comparable. The presented data can therefore be interpreted as the effect of dispersed asphaltenes on wax crystallization.

In DSC analysis, the qualitative shape of the exothermic peak due to wax crystallization was similar for all samples. As depicted in Fig. 10, the main difference between the samples is crystallization onset at a different temperature. Shifts could also occur at a later stage of crystallization, such as the heat profile of *bulk* asphaltenes. There, the heat flow in comparison to other samples appears higher between 20 and 0 °C, and lower after 0 °C. Paraffin wax crystallization consequently can be affected during all stages of crystallization.

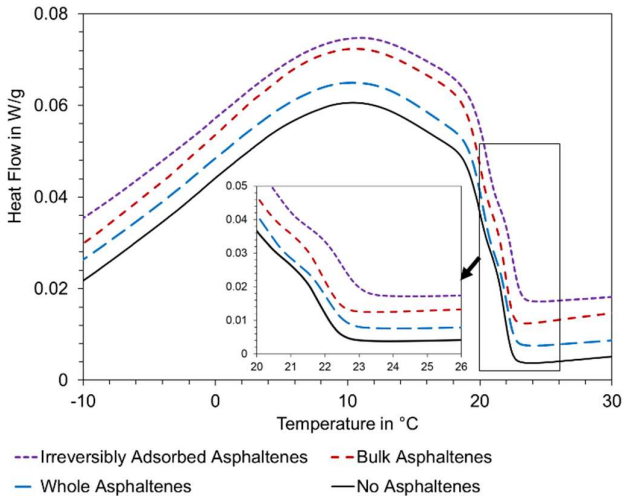

Fig. 10. DSC heat flow versus temperature at a cooling rate of 5 °C/min for four selected samples of 1500 ppm asphaltenes and 10 wt% macrocrystalline wax in xylene isomer blend. Graphs were shifted on the y-axis for better overview.

As shown in Fig. 11, the effect on WAT_0 was the greatest for *bulk* asphaltenes, which is in agreement with other reports [6, 29, 34]. *Irreversibly adsorbed* asphaltenes accounted for no measurable change in WAT_0. This indicates that there is either no effect or that positive and negative effects are cancelling out. The second lowest effect on WAT_0 was displayed by *3.5V* asphaltenes. These two fractions have poor solubility and a higher oxygen content in common. Gel breakage strength was lowered the most by *whole*, *3.5V*, and *3.5V-6V* asphaltenes. Fractionation on calcium carbonate yielded asphaltene groups, which all had less or no effect on gel breakage.

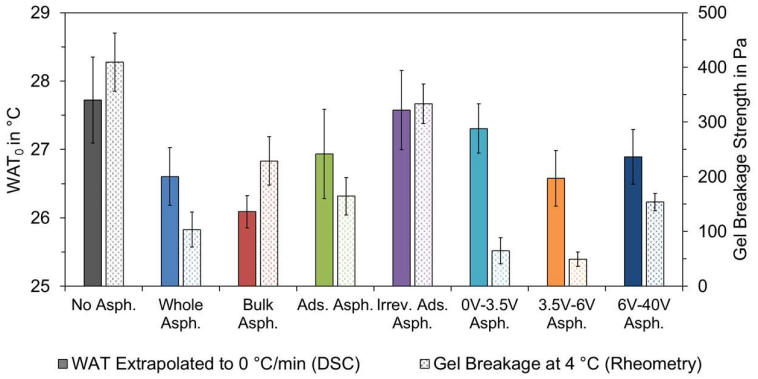

Fig. 11. Influence of different asphaltene fractions on WAT_0 and gel breakage. Measurements were done with 1500 ppm asphaltenes and 10 wt% macrocrystalline wax in xylene isomer blend. The WAT_0 was obtained via linear extrapolation from cooling rates between 0.5 °C/min and 2 °C/min with four measurements per cooling rate, yielding 16 measurements per WAT_0. Gel breakage strength was calculated as the maximum yield stress recorded during gel breakage with four to six measurements per sample. Error bars represent the standard deviation of each value.

The influence of four selected asphaltene fractions on crystal morphology is shown in Fig. 12. *Bulk* asphaltenes had less effect on crystal size than *whole* asphaltenes. The addition of *3.5V-6V* asphaltenes increased crystal distortion considerably. The effect of *3.5V* asphaltenes was similar to *3.5V-6V* asphaltenes. Other fractions not shown in Fig. 12 were also tested in CPM, but did not yield notable changes in crystal morphology as compared to *whole* asphaltenes. *Irreversibly adsorbed* asphaltenes changed crystal morphology the most. The resulting gel contained smaller, and more finely dispersed wax particles. Still, this change was not beneficial as the gel strength of *irreversibly adsorbed* asphaltenes was highest of all fractions. It has been suggested that asphaltenes act as connectors between wax crystals [30]. This could explain the comparably high gel strength for *irreversibly adsorbed* asphaltenes, since reduction of wax crystal size usually leads to a decrease in gel strength. These asphaltenes might be incorporated into the wax crystals via co-precipitation, while the polar sections could act as connectors between the crystals. This could then form an interconnected and volume spanning network of higher strength.

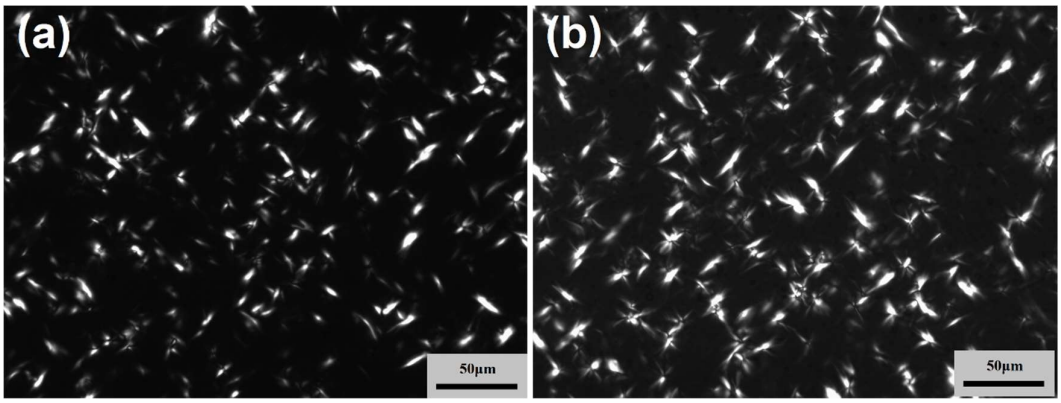

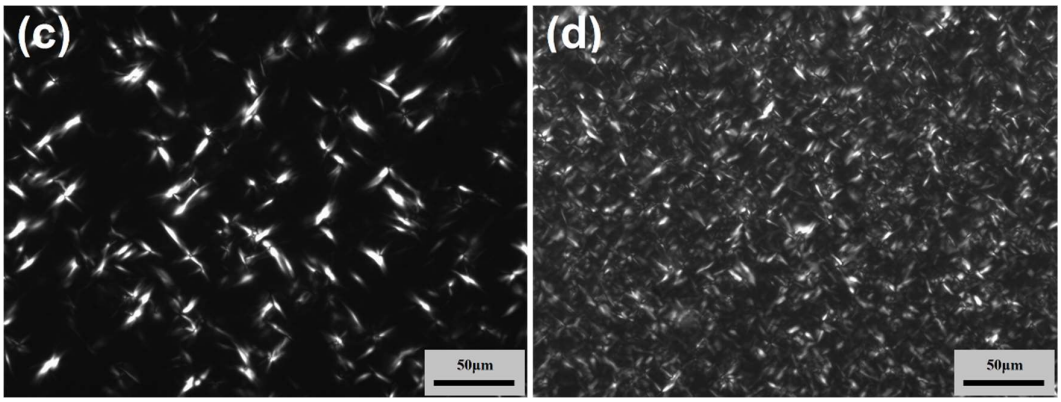

Fig. 12. CPM images of 10 wt% macrocrystalline wax in xylene isomer blend with (a) 1500 ppm whole asphaltenes, (b) 1500 ppm 3.5V-6V asphalenes, (c) 1500 ppm bulk asphaltenes, and (d) 1500 ppm irreversibly adsorbed asphaltenes

WAT and pour point are both measures that describe particular instances during wax crystallization. Asphaltenes can delay certain aspects of wax crystallization based on their composition. As a result, decreases in WAT and pour point follow a similar trend for each asphaltene fraction. Fig. 13 reveals that *bulk* asphaltenes had the greatest influence on both measures. *Irreversibly adsorbed* asphaltenes showed no detectable change in WAT and pour point compared to no asphaltenes. The remaining asphaltene fractions all accounted for decreases in WAT and pour point, and were within the standard deviation similar to the effect of *whole* asphaltenes.

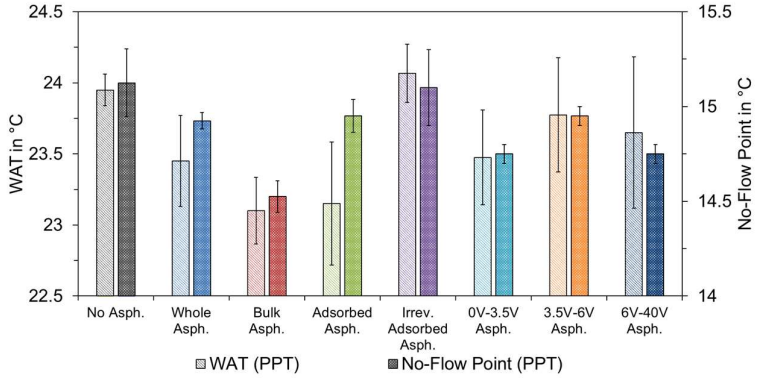

Fig. 13. Influence of different asphaltene fractions on WAT and No-Flow Point. Measurements were done with 1500 ppm asphaltenes and 10 wt% macrocrystalline wax in p-xylene using a pour point tester (PPT). Each value represents the average of 2 to 4 measurements with according standard deviation as error bars.

Separation via adsorption on calcium carbonate also represents a separation based on polarity, due to the polar nature of adsorbent, and eluents with different polarities. As a consequence, *bulk* asphaltenes can be considered less polar, and *irreversibly adsorbed* asphaltenes can be considered more polar than *whole* asphaltenes. Overall, this separation did not yield a product with improved wax inhibition performance. *Bulk* asphaltenes showed the best results in terms of WAT and pour point. Still, this fraction had less effect on gel breakage strength and crystal morphology than *whole* asphaltenes. Averaged over all five parameters, *3.5V*, and *3.5V-6V* asphaltenes showed the best effect. Both fractions had a higher impact on gel breakage strength and crystal morphology than *whole* asphaltenes, and accounted for similar or better pour point depression. Only the effect on WAT was similar to or poorer than that of *whole* asphaltenes. Low solubility therefore could be advantageous. This complies with research suggesting that less soluble asphaltenes are often found in wax deposits [32]. Also, low solubility could facilitate co-precipitation with wax, which is a requirement for crystal modifiers. Morphological changes in the wax crystal could further be induced by polar functional groups in the asphaltene molecules. As CPM imaging showed, the degree of crystal distortion is highest for

irreversibly adsorbed asphaltenes and lowest for *bulk* asphaltenes. Still, crystal distortion and gel strength did not correlate. Regarding gel strength, the best results were obtained from the second fraction, respectively, *adsorbed* and *3.5V-6V* asphaltenes. A counter intuitive trend is given by the development of H/C ratio with inhibition performance for asphaltenes from bulk precipitation. Lower solubility fractions, i.e. *3.5V* asphaltenes, have higher H/C ratios, which indicates more aromatic and less aliphatic systems. The aliphatic part of an asphaltene molecule is considered responsible for asphaltene-wax interactions. Still the products from bulk fractionation showed better effect on wax crystal morphology and gel yield strength for fractions with supposedly higher aromaticity. An explanation could be that other effects, such as the influence of asphaltene solubility, are counteracting the change in aliphatic content.

At the bottom line, none of the fractionation procedures isolated asphaltenes that could be an alternative to polymeric PPDs. The fractions from adsorption on calcium carbonate even showed on average lower performance than the original material, *whole* asphaltenes. This indicates that asphaltenes of different properties and functional groups might need to act synergistically to have a good effect on wax crystallization. Another explanation would be that the chemical composition of the asphaltenes has been altered, which is supported e.g. by the increase in oxygen content in Table 2. All in all, the results indicate that low solubility and intermediate polarity have the most favorable effect on wax crystallization.

3.4. Asphaltene-Wax Interactions

Asphaltene-wax interactions were measured via ITC using solutions of 2 wt% asphaltenes in xylene isomer blend. This concentration was considered high enough for good signal response, but low enough to prevent asphaltene precipitation in the syringe. ITC experiments were made with *bulk* and *irreversibly adsorbed* asphaltenes to include fractions of the highest and lowest polarity. *Whole* asphaltenes were also tested to compare with the original material. Injections were made into a 10 wt% macrocrystalline wax in xylene isomer blend. Random checks were performed with a microscope on asphaltene solutions. At no point were particle flocculates found. The presented data therefore accounts for interactions of dispersed asphaltenes, i.e. most likely nanoaggregates, with wax. ITC experiments conducted at 35 °C contained solubilized wax only, and typical results are shown in Fig. 14. The precipitation onset of the waxy solution was measured to be WAT_0 = 27.7 °C. At 20 °C, a fraction of macrocrystalline wax had therefore precipitated. Results of ITC experiments conducted at 20 °C are plotted in Fig. 15.

The heat profile of every injection shows a large minimum and subsequent return to the baseline. Secondary effects can be observed for *whole* and *irreversibly adsorbed* asphaltenes in Fig. 14, where local extrema on a scale of less than 1% of the large minimum are visible in the heat profile approximately 5 to 10 min after each injection. It appears that multiple processes are taking place, which have different kinetics. Similarly, local minima or inflection points can be observed that follow the minimum right after each injection in Fig. 15. At both temperatures, the largest heat contributor is the dilution or re-dissolution of wax. This process as well as asphaltene dissociation are endothermic reactions. Consequently, as the heat released is lower in presence of asphaltenes, an exothermic reaction between asphaltenes and wax can be observed in Fig. 14 and Fig. 15. Also visible is the difference in time scale. Experiments at 35 °C showed a comparably fast return to the baseline after each injection. The injection interval could therefore be set at 15 min and less. Experiments at 20 °C accounted for a slower return to the baseline. It appears that the involved re-dissolution processes of solid wax are rate limiting. Injection intervals were set at 60 min. Complete equilibration at the end of each injection interval is not the case. Still, the experiments showed good reproducibility, little to no baseline drift, and equilibration during early injections. Because of that, the injection interval was not increased. Too

long injection intervals promote the influence of solvent evaporation and diffusion into the syringe tip, so this decision is always a tradeoff.

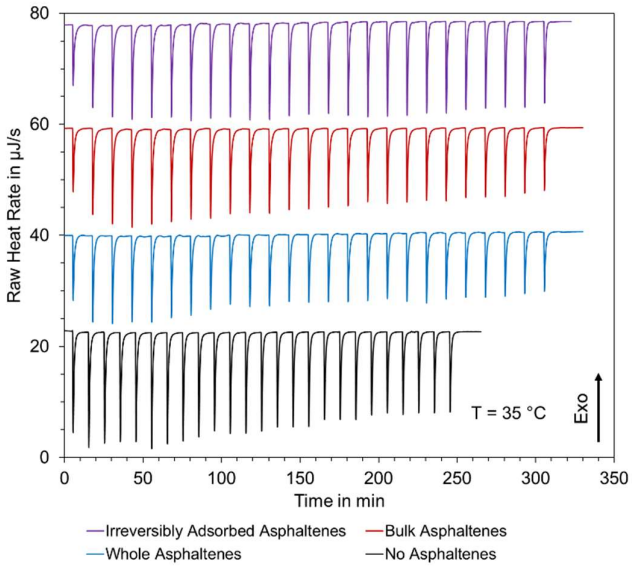

Fig. 14. ITC heat profiles for 25 injections of 2 wt% asphaltenes into 10 wt% macrocrystalline wax in xylene isomer blend at 35 °C. Graphs have been shifted on the y-axis for better overview.

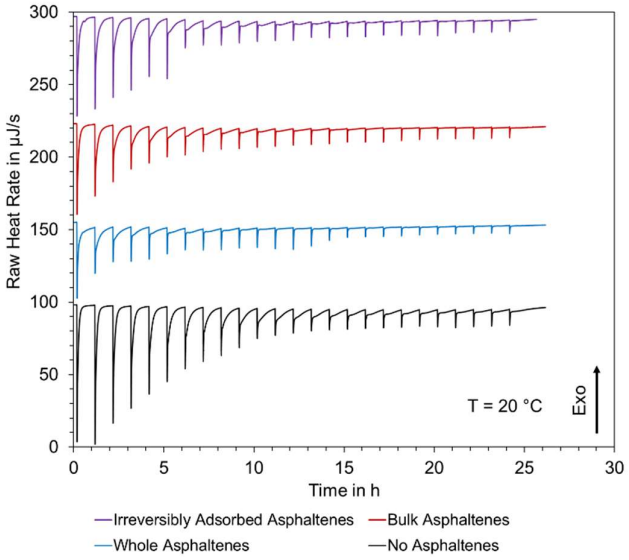

Fig. 15. ITC heat profiles for 25 injections of 2 wt% asphaltenes into 10 wt% macrocrystalline wax in xylene isomer blend at 20 °C. Graphs have been shifted on y-axis for better overview.

The heat released during each titration is computed by integration. For this, a linear baseline is fitted between each injection point. The calculated interaction heat for *whole*, *bulk*, and *irreversibly adsorbed* asphaltenes with macrocrystalline wax is plotted in Fig. 16 and Fig. 17. The contributions ΔH_{Total}, ΔH_{Asph}, and ΔH_{Wax} are the average of two to four measurements, depending on reproducibility of the individual value. Results for *whole* asphaltenes have been published previously [49], but were measured two additional times to provide higher statistical significance.

For experiments conducted at 35 °C in Fig. 16, the resulting interaction heat is almost identical. All samples show maximum interaction heat at the second injection. Subsequent injections decrease in

interaction heat and asymptotically approach zero interaction heat towards the final injections. *Bulk* asphaltenes are on average lower than *whole* and *irreversibly adsorbed* asphaltenes. Still, only during injection 3 to 5 this difference is large enough to be statistically valid.

For experiments at 20 °C in Fig. 17, the interaction heat per injection is by a factor of 10 to 45 higher than at 35 °C. Interactions of asphaltenes with solid wax appear to be stronger than with dissolved wax. *Bulk* and *irreversibly adsorbed* asphaltenes are within the standard deviation similar in interaction heat at 20 °C. *Whole* asphaltenes are considerably higher in interaction heat during injection 3 to 10. All samples have a global maximum at either injection 8 or 9. Towards the final injections all samples are converging and asymptotically approach zero interaction heat. This could be explained by a diminishing of reaction sites at the end. Interactions with both dissolved and solid wax are exothermic, as the interaction heat attained negative heat values.

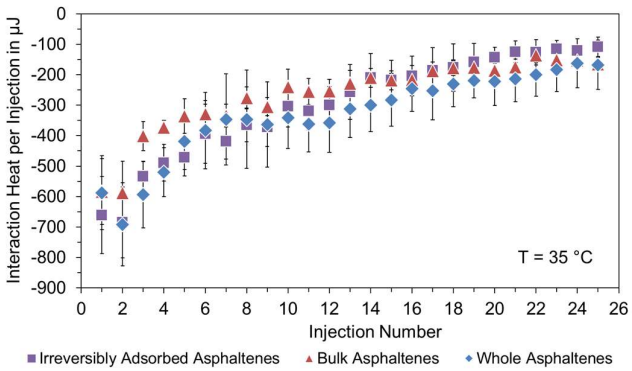

Fig. 16. Interaction heat for 2 wt% asphaltenes with 10 wt% macrocrystalline wax in xylene isomer blend at 35 °C. The wax is fully in solutions, as WAT_0 = 27.7. Error bars represent the standard deviation.

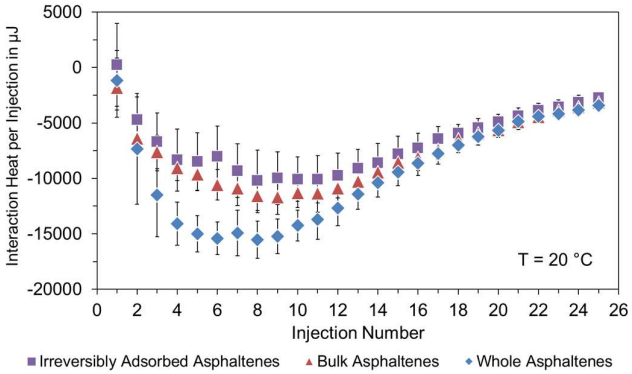

Fig. 17. Interaction heat for 2 wt% asphaltenes with 10 wt% macrocrystalline wax in xylene isomer blend at 20 °C. The wax is partially crystallized, as WAT_0 = 27.7 °C. Error bars represent the standard deviation.

It can be concluded that separation on calcium carbonate did not produce a fraction with increased interaction heat. On the contrary, interactions with solid wax were highest for unfractionated *whole* asphaltenes. Interactions with solubilized wax did not show significant difference between the tested samples. Neither the most polar *irreversibly adsorbed* asphaltenes, nor the least polar *bulk* asphaltenes interact more strongly with macrocrystalline wax. Instead, *whole* asphaltenes with intermediate polarity accounted for the strongest interactions with solid wax. It appears that the sum of all functional groups contribute more to asphaltene-wax interactions than one group with more distinct properties. These results are concurring with section 3.3, where the best effects on crystal morphology and waxy gel strength were achieved by asphaltenes with a mixed range of functional groups.

4. Conclusion

This article investigated the effect of fractionated asphaltenes on wax crystallization. Asphaltenes were separated into groups with more distinct properties via adsorption on calcium carbonate or stepwise precipitation with *n*-hexane. A waxy model oil containing macrocrystalline wax in xylene was used to study the effect of asphaltenes on wax crystallization. The performance of asphaltenes to act as WIs was investigated via DSC, rheometry, CPM, and PPT. Asphaltene-wax interactions were measured in ITC. Key results are summarized as follows.

1. In experiment design, asphaltene concentrations and solvent were chosen to provide stable asphaltene nano-aggregates without flocculation. According to FTIR spectra, all asphaltene fractions displayed abundance of aliphatic groups, which can facilitate co-crystallization with wax.
2. Increasing the concentration of *whole* asphaltenes facilitated changes to wax crystal morphology and decreased gel yield strength. Regarding WAT and pour point, a concentration increase did not always yield an improvement.
3. Fractionation on calcium carbonate resulted in asphaltene groups with the largest differences in composition and properties. Yet, the overall inhibition performance and interaction strength of each group with wax did not improve as compared to unfractionated *whole* asphaltenes.
4. *Bulk* asphaltenes from fractionation on calcium carbonate induced the largest WAT and pour point decreases. Still, the effect on gel yield strength and crystal morphology was less pronounced. This group had lower polarity and the lowest H/C ratio indicating higher amounts of aromatic structures.
5. *Irreversibly adsorbed* asphaltenes accounted for the largest changes in crystal morphology, forming smaller and finely dispersed wax crystals. Still, wax inhibition performance was poor in terms of pour point and waxy gel strength. This fraction contained increased quantities of carbonyl, carboxylic or derivative groups, making it the highest polarity group.
6. Solvent fractionation resulted in the fractions *3.5V, 3.5V-6V*, and *6V-40V* asphaltenes, which differed in solubility, but had more similar composition and functional groups than asphaltenes from fractionation on calcium carbonate. The groups *3.5V* and *3.5V-6V* asphaltenes showed the best effect on waxy gel strength and similar or better pour point depression as compared to *whole* asphaltenes.

Overall, asphaltene fractionation did not yield a product equivalent to polymeric PPDs. Wax inhibition performance tended to be best for asphaltene fractions with low solubility and a mixed range of functional groups. Wax crystallization is therefore influenced by an ensemble of asphaltenes with different properties. It is suggested that asphaltenes with different chemical compositions might form synergies when acting on wax crystallization. These synergies could be explained by bi-functional colloids: Less polar asphaltenes interact with wax i.e. by facilitating co-crystallization, whereas more polar asphaltenes impose spatial interferences during wax crystal growth. This would result in the formation of more distorted wax crystals with less propensity to interlock. Still, additional data is needed to support this hypothesis, e.g. the precise structure and composition of individual asphaltene molecules.

5. Acknowledgements

This work was carried out as a part of SUBPRO, a Research-based Innovation Centre within Subsea Production and Processing. The authors gratefully acknowledge the financial support from SUBPRO, which is financed by the Research Council of Norway, major industry partners and NTNU.

6. Acronyms

CPM = cross-polarized microscopy

DCM = dichloromethane

DSC = differential scanning calorimetry

FTIR = Fourier-transformed infrared spectrometry

ITC = isothermal titration calorimetry

MAC = maleic anhydride co-polymer

NIR = near-infrared spectroscopy

PEB = poly(ethylene-butene)

PPD = pour point depressant

PPT = pour point tester

QCM = quartz crystal microbalance

THF = tetrahydrofuran

WAT = wax appearance temperature

WI = wax inhibitor

7. References

1. Kelland, M.A., *Production chemicals for the oil and gas industry*. second ed. 2014, Boca Raton: CRC press.
2. Aiyejina, A., et al., *Wax formation in oil pipelines: A critical review.* International Journal of Multiphase Flow, 2011. **37**(7): p. 671-694.
3. Paso, K.G., *Paraffin gelation kinetics*. 2005: University of Michigan.
4. Prahl, U., *Isolierung erdölstämmiger Pour Point Depressants und Untersuchung ihrer Wirkungsweise in paraffinhaltigen Fluiden*, in *Fakultät für Bergbau, Hüttenwesen und Maschinenwesen*. 2001, Technische Universität Clausthal: Papierflieger.
5. Tinsley, J.F., et al., *Waxy Gels with Asphaltenes 1: Characterization of Precipitation, Gelation, Yield Stress, and Morphology.* Energy & Fuels, 2009. **23**(4): p. 2056-2064.
6. Venkatesan, R., et al., *The Effect of Asphaltenes on the Gelation of Waxy Oils.* Energy & Fuels, 2003. **17**(6): p. 1630-1640.
7. Jensen, H.P., *Pour point depressant made from the asphaltene component of thermally treated shale oil*, U.S.P.a.T. Office, Editor. 1980, Chevron Research Company, San Francisco, Calif.: USA.
8. Wunderlich, D.K. and J.H. Frankovich, *Pour point depressant made by hydrovisbreaking and deasphalting a shale oil*, U.S.P. Office, Editor. 1970, Sinclair Oil Corporation, New York: USA.
9. Irving, G.B. and E. Knapp, *Process for reducing the pour point of shale oil*, U.S.P. Office, Editor. 1970, Esso Research and Engineering Company: USA.
10. Subramanian, S., et al., *Asphaltene fractionation based on adsorption onto calcium carbonate: Part 1. Characterization of sub-fractions and QCM-D measurements.* Colloids and Surfaces A: Physicochemical and Engineering Aspects, 2016. **495**: p. 136-148.
11. Subramanian, S., et al., *Asphaltene fractionation based on adsorption onto calcium carbonate: Part 2. Self-association and aggregation properties.* Colloids and Surfaces A: Physicochemical and Engineering Aspects, 2017. **514**: p. 79-90.

12. Machado, A.L.d.C. and E.F. Lucas, *Poly(Ethylene-co-Vinyl Acetate) (EVA) Copolymers as Modifiers of Oil Wax Crystallization.* Petroleum Science and Technology, 1999. **17**(9-10): p. 1029-1041.
13. Huang, Z., S. Zheng, and H.S. Fogler, *Wax Deposition: Experimental Characterizations, Theoretical Modeling, and Field Practices*. 2015, Boca Raton: CRC Press.
14. Paso, K., et al., *Paraffin Polydispersity Facilitates Mechanical Gelation.* Industrial & Engineering Chemistry Research, 2005. **44**(18): p. 7242-7254.
15. Rahimian, I., H. Laux, and H.-J. Oschmann, *Trübungs-und Stockpunktabhängigkeiten in Erdölen.* Erdöl, Erdgas, Kohle, 1997. **113**(2): p. 80-83.
16. Clarke, E.W., *Crystal Types of Pure Hydrocarbons in the Paraffin Wax Range.* Industrial & Engineering Chemistry, 1951. **43**(11): p. 2526-2535.
17. Yang, F., et al., *Polymeric Wax Inhibitors and Pour Point Depressants for Waxy Crude Oils: A Critical Review.* Journal of Dispersion Science and Technology, 2015. **36**(2): p. 213-225.
18. Zhao, Y., *Shut in and Restart of Waxy Crude Oil Pipelines: Gelation, Rheology Model Development, and Application of Polymer/Ionic Liquid Based Additive*. 2013, Tondheim, Norway: Norges teknisk-naturvitenskapelige universitet (NTNU).
19. International, A., *Standard Test Method for Pour Point of Petroleum Products*, in *D97*. 2017.
20. Wei, B., *Recent advances on mitigating wax problem using polymeric wax crystal modifier.* Journal of Petroleum Exploration and Production Technology, 2015. **5**(4): p. 391-401.
21. Machado, A.L.C. and E.F. Lucas, *Influence of ethylene-co-vinyl acetate copolymers on the flow properties of wax synthetic systems.* Journal of Applied Polymer Science, 2002. **85**(6): p. 1337-1348.
22. Oschmann, H.-J., *Das Kristallisationsverhalten von Paraffinen in Abhängigkeit von ihrer Zusammensetzung sowie seine Beeinflussung durch Paraffininhibitoren*, in *Fakultät für Bergbau, Hüttenwesen und Maschinenwesen*. 1998, Technische Universität Clausthal: Papierflieger.
23. Oliveira, G.E., et al., *The Effect of Asphaltenes, Naphthenic Acids, and Polymeric Inhibitors on the Pour Point of Paraffins Solutions.* Journal of Dispersion Science and Technology, 2007. **28**(3): p. 349-356.
24. García, M.d.C. and L. Carbognani, *Asphaltene−Paraffin Structural Interactions. Effect on Crude Oil Stability.* Energy & Fuels, 2001. **15**(5): p. 1021-1027.
25. Tinsley, J.F., et al., *Waxy Gels with Asphaltenes 2: Use of Wax Control Polymers.* Energy & Fuels, 2009. **23**(4): p. 2065-2074.
26. Yao, B., et al., *Ethylene–Vinyl Acetate Copolymer and Resin-Stabilized Asphaltenes Synergistically Improve the Flow Behavior of Model Waxy Oils. 2. Effect of Asphaltene Content.* Energy & Fuels, 2018.
27. Yao, B., et al., *Ethylene–Vinyl Acetate Copolymer and Resin-Stabilized Asphaltenes Synergistically Improve the Flow Behavior of Model Waxy Oils. 1. Effect of Wax Content and the Synergistic Mechanism.* Energy & Fuels, 2018. **32**(2): p. 1567-1578.
28. Oh, K. and M. Deo, *Characteristics of Wax Gel Formation in the Presence of Asphaltenes.* Energy & Fuels, 2009. **23**(3): p. 1289-1293.
29. Alcazar-Vara, L.A., J.A. Garcia-Martinez, and E. Buenrostro-Gonzalez, *Effect of asphaltenes on equilibrium and rheological properties of waxy model systems.* Fuel, 2012. **93**: p. 200-212.
30. Lei, Y., et al., *Study on the Effect of Dispersed and Aggregated Asphaltene on Wax Crystallization, Gelation, and Flow Behavior of Crude Oil.* Energy & Fuels, 2014. **28**(4): p. 2314-2321.
31. Lei, Y., S. Han, and J. Zhang, *Effect of the dispersion degree of asphaltene on wax deposition in crude oil under static conditions.* Fuel Processing Technology, 2016. **146**: p. 20-28.
32. Rogel, E., et al., *Asphaltene characterization of paraffinic crude oils.* Fuel, 2016. **178**(Supplement C): p. 71-76.

33. Song, X., et al., *Effect of SiO2 Nanoparticles on Wax Crystallization and Flow Behavior of Model Crude Oil.* Industrial & Engineering Chemistry Research, 2016. **55**(23): p. 6563-6568.
34. Li, Y., et al., *Influence of Asphaltene Polarity on Crystallization and Gelation of Waxy Oils.* Energy & Fuels, 2018. **32**(2): p. 1491-1497.
35. Ariza-León, E., D.-R. Molina-Velasco, and A. Chaves-Guerrero, *Review of Studies on Asphaltene - Wax Interaction and the Effect thereof on Crystallization.* CT&F - Ciencia, Tecnología y Futuro, 2014. **5**: p. 39-53.
36. Yang, X. and P. Kilpatrick, *Asphaltenes and Waxes Do Not Interact Synergistically and Coprecipitate in Solid Organic Deposits.* Energy & Fuels, 2005. **19**(4): p. 1360-1375.
37. García, M.d.C., *Crude Oil Wax Crystallization. The Effect of Heavy n-Paraffins and Flocculated Asphaltenes.* Energy & Fuels, 2000. **14**(5): p. 1043-1048.
38. Kokal, S.L. and S.G. Sayegh, *Asphaltenes: The Cholesterol Of Petroleum*, in *Middle East Oil Show*. 1995, Society of Petroleum Engineers: Bahrain.
39. Kriz, P. and S.I. Andersen, *Effect of Asphaltenes on Crude Oil Wax Crystallization.* Energy & Fuels, 2005. **19**(3): p. 948-953.
40. Orea, M., et al., *Retention of Alkane Compounds on Asphaltenes. Insights About the Nature of Asphaltene–Alkane Interactions.* Energy & Fuels, 2016. **30**(10): p. 8098-8113.
41. Kaminski, T.J., et al., *Classification of Asphaltenes via Fractionation and the Effect of Heteroatom Content on Dissolution Kinetics.* Energy & Fuels, 2000. **14**(1): p. 25-30.
42. Paso, K., et al., *Wax Deposition Investigations with Thermal Gradient Quartz Crystal Microbalance*, in *Handbook of Surface and Colloid Chemistry*. 2009, CRC Press. p. 567-584.
43. Pinto, F.E., et al., *Fractionation of asphaltenes in n-hexane and on adsorption onto CaCO3 and characterization by ESI(+)FT-ICR MS: Part I.* Fuel, 2017. **210**: p. 790-802.
44. Ruwoldt, J., M. Kurniawan, and H.-J. Oschmann, *Non-linear dependency of wax appearance temperature on cooling rate.* Journal of Petroleum Science and Engineering, 2018. **165**: p. 114-126.
45. International, A., *Standard Test Method for Pour Point of Petroleum Products (Rotational Method)*, in *D5985*. 2014.
46. Wei, D., et al., *Aggregation of tetrameric acid in xylene and its interaction with asphaltenes by isothermal titration calorimetry.* Journal of Thermal Analysis and Calorimetry, 2015. **122**(1): p. 463-471.
47. Zhao, Y., et al., *Gelation and Breakage Behavior of Model Wax–Oil Systems: Rheological Properties and Model Development.* Industrial & Engineering Chemistry Research, 2012. **51**(23): p. 8123-8133.
48. Paso, K.G., *Comprehensive treatise on shut-in and restart of waxy oil pipelines.* Journal of Dispersion Science and Technology, 2014. **35**(8): p. 1060-1085.
49. Ruwoldt, J., et al. *Isothermal Titration Calorimetry for Assessing Wax-Inhibitors*. in *Chemistry in the Oil Industry XV: Enabling Efficient Technologies Programme*. 2017. Manchester (UK).